Parametric Surfaces with Volume of Solid Control for Optimisation of Three Dimensional Aerodynamic Topologies

A. D. J. Payot * ; T. C. S. Rendall † ; C. B. Allen ‡
Department of Aerospace Engineering, University of Bristol, Bristol, UK

This paper presents a topologically flexible parameterisation method suitable for the optimisation of 3 dimensional aerodynamics using traditional boundary fitted meshes. This parameterisation extends the restricted-snake volume of solid (RSVS) parameterisation previously developed by the authors. This is achieved by extending restricted snakes, a parametric active contour method, into a restricted surface capable of efficiently evolving arbitrary complex topologies handling collisions with no floating point arithmetic. This is integrated with a surface generation rule which allows smooth shapes with intuitive parameterisation of topology. The 3D-RSVS is presented along with results displaying its smooth behaviour, it's ability to produce shapes of aerodynamic interest and it's topological flexibility. A hierarchical approach to the volume of solid design variables is presented for the RSVS, allowing automatic design of the grids on which VOS are specified. An optimisation framework is proposed and some example 2 dimensional optimisation results are presented.

I. Introduction

Increases in computational power and improvements in computational fluid dynamics (CFD) tools have created the possibility of using CFD-based optimisation in industrial design. By allowing a systematic and unbiased exploration of a design space, optimisation methods can be used to expand a designer's understanding of the problem being tackled, allowing better overall aerodynamic performance. As designers look to improve performance, aircraft manufacturers are turning increasingly to numerical optimisation. Frameworks for aerodynamic optimisation require the integration of parameterisation methods, mesh generators and flow solvers with optimisation methods. The tendency in this has been to use a modular approach by integrating established modelling and CFD packages with existing optimisers.

The complexity of parameterisation arises from the different origins of optimisation methods and CFD processes. Optimisation methods are mathematical algorithms devised to find the extrema of functions, and have rigorous mathematical underpinnings, while CFD originated from the need to evaluate the aerodynamic properties of potential designs. The translation of the mathematical formulations used by optimisers into the geometric designs used by CFD is a complex problem with implications on the efficiency and effectiveness of optimisation frameworks. Parameterisation methods need to be compact (using few design variables) while not artificially limiting the geometric shapes that can be represented [1]. This focus led to aerodynamic optimisation methods capable of efficiently handling small surface changes, without allowing larger and more complex topological changes in geometries.

In structural design the benefits of exploring different topologies is key to generating light-weight and efficient structures. The field of numerical structural topology optimisation (STO) has been an active field of research for the last 30 years and it has recently seen industrial application on the Boeing CH-47 Chinook and the Airbus A380; it allowed a weight reduction of 17% of underfloor beams compared to a conventional structural optimisation method [2] on the CH-47 and weight reduction of the leading edge droop ribs on the A380. This effort in the finite elements (FE) community has led to parameterisation methods able to represent complex topologies with a single set of design variables [3–5].

The justification for topological optimisation is straightforward in structural applications, from truss space-frames to honeycomb designs, there are a wide range of possible engineering structures; furthermore a structural member's impact is readily summarised to a set of interactions at its boundary. The possibility to reduce designs to a set of external interactions and the Lagrangian formulation of CSD solvers facilitates the implementation of structural topological optimisation within existing designs.

There is no such separation in aerodynamics; the aerodynamic shape is intrinsically linked to the rest of the design by its need to be supported by an underlying structure. This means that aerodynamic topological optimisation of an entire aircraft or wing is unlikely to be a reality in the near or medium term. However, there is scope for the

*PhD Student, AIAA Student Member, a.payot@bristol.ac.uk, Bristol, BS8 1TR, UK
†Lecturer, AIAA Member, thomas.rendall@bristol.ac.uk, Bristol, BS8 1TR, UK
‡Professor of Computational Aerodynamics, AIAA Senior Member, c.b.allen@bristol.ac.uk, Bristol, BS8 1TR, UK

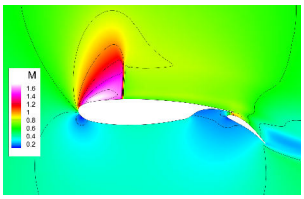

a) C_P plot of a two element aerofoil.

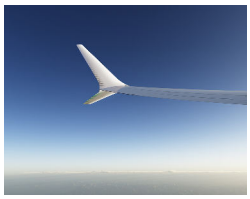

b) Winglet of the Boeing 737-MAX (Boeing).

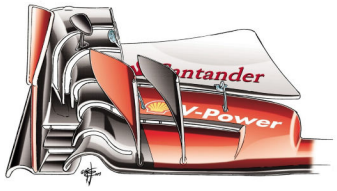

c) Front wing of the SF-15 Ferrari F1 car (Giorgio Piola).

d) Eagle in flight.

Figure 1. Examples of complex topology in aerodynamic applications (Sources: fig.1b - Wing tip[a]; fig.1c - F1 front wing[b])

aerodynamic topological optimisation of local features; topological optimisation of wing tips would allow feathered or split winglets more complex than that on the Boeing 737-MAX to be explored (fig. 1b and fig. 1d). No current optimisation framework for external aerodynamics supports the exploration of 3-dimensional topological changes, because none of the parameterisation methods commonly in use can represent different topologies with a single set of design variables.

An effective topological aerodynamic optimisation framework offers the possibility of radically new designs. Applications to Formula 1 (fig. 1c), unmanned aerial vehicles, commercial strut-braced wing design and internal engine design could offer significant improvements in performance. This paper presents the development of a parameterisation method which can handle topology changes while maintaining a compact design space, allowing the exploration of new aerodynamic optimisation problems.

A. Existing Aerodynamic and Structural Optimisation Methods

Earlier developments in the field of parameterisation for aerodynamics have yielded a wealth of different methods for the representation of aerodynamic designs. Parameterisation methods can be separated broadly in two categories: constructive and deformative methods. Constructive methods define completely the geometry from the set of design variables; these include B-Spline and polynomial interpolation [6] in general, and CST [7] and PARSEC [8] in particular. Deformative methods by comparison define a set of modifications to a baseline geometry; notable among these are the Hicks-Henne bump functions [9], Singular Value Decomposition (SVD) deformation modes [10, 11] and Free-Form Deformation (FFD) methods [12, 13]. While most parameterisations presented here can be extended to three dimensions, their capability varies widely. In three dimensions a common approach is to use FFD deformation methods as these can be adapted to work directly on an existing mesh.

Previous systematic investigations by Vassberg et al. [1, 14] have highlighted the impact of dimensionality on the drag minimisation of a standard test case, showing the importance of geometric flexibility while maintaining a compact set of design variables. Work by Castonguay and Nadarajah [15], and more recently by Masters et al. [16, 17] has compared the impact of established parameterisation methods on geometric flexibility, pressure distribution recovery and optimal drag results. These studies show that effective parameterisation methods will require few design variables while providing smooth control of the aerodynamic profile. Smooth control is achieved when a small change in the numerical representation leads to a similarly small change in the represented geometry. This requirement results from the expense associated with converging optimisers in large design spaces, balanced against the need to not artificially restrict the scope of geometries that can be represented [1].

Most aerodynamic parameterisation methods to date have focused on producing smooth designs with small numbers of design variables. One key geometric restriction that affects all established parameterisation methods is the inability to transition between topologies. What this means is that no conventional aerodynamic optimisation framework for external large scale flows is currently capable of exploring the number of aerodynamic bodies with a single set of design variables. This article presents an aerodynamic parameterisation with this topological flexibility.

In structural topology optimisation homogenisation and level set methods have been used to tackle complex topological optimisation problems in two and three dimensions; however these structural methods have limitations in terms of their application to aerodynamics. The first methods developed for STO were *homogenization methods*; these rely

[a]Courtesy of Boeing available at: http://www.boeing.com/commercial/737max/#/design-highlights/max-efficiency/max-at-winglet/ accessed on: 05/04/2017

[b]Courtesy of Giorgio Piola available at: https://www.formula1.com/content/fom-website/en/latest/technical/2015/9/ferrari-sf15-t---low-downforce-front-wing/_jcr_content/featureContent/manual_gallery/image1.img.2048.medium.jpg/1441192443879.jpg accessed on: 05/04/2017

on the segmentation of the design domain into squares in which the density of a material can be varied to change a design's weight and local load carrying ability. By affecting directly the density of the material in the discretisation of the structural solver homogenization methods do away completely with the need for an explicit representation of a profile. These works led to the development of the solid isotropic material with penalisation (SIMP) method [18], the most widely used STO procedure. Homogenization methods do not maintain a representation of the outer boundary of the shape and instead rely on direct interaction with the structural solver, while this can be applied in CFD in Stokes and incompressible flows at low Reynolds numbers [19–22] using finite element solvers [3]; it is not appropriate for external aerodynamics which use solutions to the Euler and Reynolds averaged Navier-Stokes (RANS) equations at high Reynolds numbers.

The main alternative to homogenization are level-set methods (LSM) introduced by Wang et al. [23]. In these methods the structural profile is represented by the level set of a parametric function. These methods were shown to be very competitive and solve some of the shortcomings of homogenization methods [23]. Level sets methods include a wide range of approaches for the definition of the level set function, each of these choices affects the behaviour of optimisation processes [24]. However these methods have in common the implicit definition of the profile and can rely on three mechanisms for change: boundary profile variations; functional parameter variations; and topological variations. To be effective these methods rely on very close integration with the optimisation method, notably by using the Hamilton-Jacobi equations to propagate the boundary of the profile as a moving front [24]. The ubiquitous availability of adjoint solutions to structural equations and the relative low cost of the solver means that the compactness of the parameterisations and the efficiency of the optimisation process are less critical than in aerodynamic applications limiting the direct use of existing methods for aerodynamics.

Some progress towards a topologically flexible external aerodynamic parametrisation has been achieved by Hall et al. [25, 26]. This method relies on material distribution, or volume of solid (VOS), to generate the external geometry of an aerodynamic body. An example of this type of design space is shown in figure 2a. The VOS approach is inspired from volume of fluid methods used in multi-fluid simulations. It is, in optimisation terms, conceptually similar to homogenization methods: it defines explicitly regions of space which are full or empty based on a predefined grid. In each cell of this grid the fraction of that cell which must be inside the profile is specified by a value between 0 and 1, this allows the parameterisation to be understood intuitively by a designer. The VOS method by Hall et al. [25] uses this information to generate a smooth level set function from which a contour that approximately matches the VOS is extracted. While effective on cases where topological flexibility was required, it underperformed compared to other aerodynamic parameterisation methods in terms of its compactness and smoothness.

B. Development of the Aerodynamic Topology Optimisation Framework

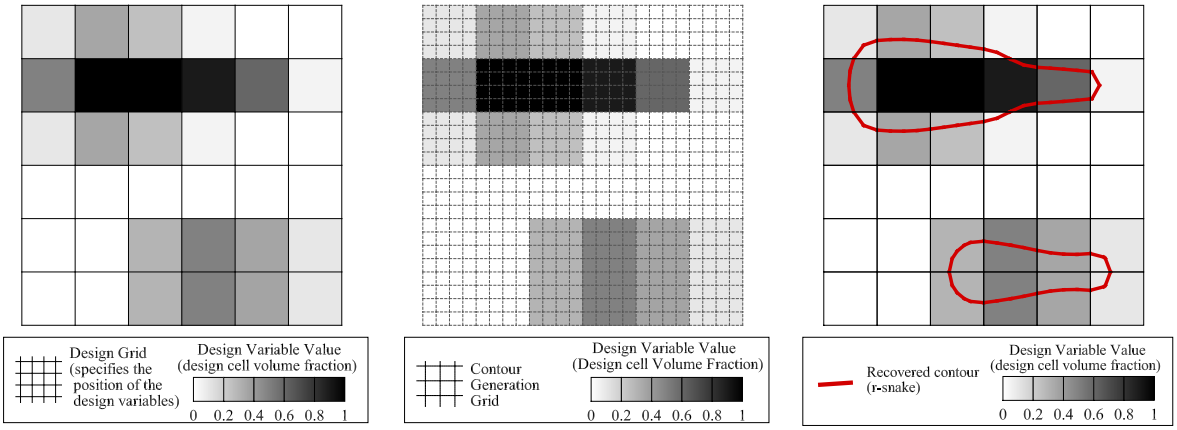

a) Example design space for the RSVS with a set of design variable values specified

b) 4 by 4 refinement of the design grid, used for contour building.

c) Contour recovered from the design variables.

Figure 2. Design grid with corresponding 4 by 4 snaking grid and an r-snake recovering a profile specified using VOS design variables.

These observations show that the development of a topological aerodynamic optimisation framework has the potential to deliver further improvements in both conventional and future aircraft configurations. This paper presents the development of the 3-dimensional restricted snake volume of solid (3D-RSVS) method, an aerodynamic parameterisation that supports topological change while performing efficiently on typical aerodynamic parameterisation and

optimisation problems. To be useful the 3D-RSVS needs to fit into current modular aerodynamic frameworks, it must have: a sufficiently compact and smooth design space; be compatible with traditional boundary fitted CFD approaches and support adjoint gradients. This is achieved by extending the 2-dimensional restricted snake volume of solid (2D-RSVS) parameterisation.

The 2D-RSVS builds upon the volumetric aerodynamic parameterisation by Hall et al. [25,26] which was the first topologically flexible parameterisation for external aerodynamics. Like the parameterisation of Hall et al., the RSVS uses volume of solid (VOS) design variables to control profile shape and topology, these were kept as they provide intuitive handling of topology change. However a contour generation method with improved geometric behaviour was developed. The 2D-RSVS is more flexible and offers a direct path to 3-dimensional parameterisation. The main challenge in this type of parameterisation is the translation of the design variables into profiles suitable for CFD analysis. This paper details how the RSVS allows to go from a VOS design space as seen in figure 2a; to a specific profile built depending uniquely on the values of the VOS design variables (fig. 2c). While this paper is focused on the development of a 3-dimensional methods, 2-dimensional figures are used to explain the parameterisation process.

In volume-based parameterisation the segmentation of volumetric information is done through a Cartesian grid, this means the design variables are best understood by a designer as grey-scale images on an underlying mesh (fig. 2a). This observation highlights the similarity between the parameterisation of geometries from volume information and the field of contour extraction in image analysis. Image segmentation, and medical image segmentation in particular, pose many of the same challenges as the volumetric parameterisation method considered earlier. The recovery of complex closed contours of arbitrary topology with limited computational expense is one that has been explored by the medical imaging community for the last 20 years. A class of methods for building such profiles that has seen significant and promising use is that of active contour methods [27, 28]. These methods rely on explicit vertex marching until the contour meets internal and external forcing conditions. Restricted snakes (r-snakes) developed by Kobbelt and Bischoff [29] are a type of parametric active contour designed to handle topology changes efficiently. These are extended into a new 3 dimesnional geometry control tool, the "restricted-surface" in section II-B. Section II-B shows how r-surfaces are used in the RSVS to generate surfaces of suitable aerodynamic quality that respect the values of VOS design variables. The shape of the r-surface is driven by equations that were found to have desirable smoothness properties, these are presented in section II-A. The 2-dimensional version of this process was used to generate the profile in figure 2c.

In addition to the r-snake and r-surface volume of solid parameterisations, significant work was carried out to understand and improve the performance of the VOS design variables used by the RSVS. Design variable smoothing processes and refinement have been developed previously to improve the behaviour of optimisation frameworks relying on the new parameterisation method [30]. Multi-level approaches to parameterisation by Anderson and Aftosmis [31] and Masters et al. [32] have shown their ability to accelerate and improve the performance of underlying optimisation frameworks. A similar hierarchical method was developed for the 2D-RSVS parameterisation in previous work by the authors [30]. This multi-level approach allowed significant performance improvements on the basic RSVS implementation in geometric and aerodynamic optimisations while removing some of the expert knowledge required when setting up new optimisation cases. Section IV explains how this process naturally extends to the 3D-RSVS to automatically produce efficient VOS design variable layouts.

This paper presents the extension of the restricted snake volume of solid (RSVS) parameterisation to 3 dimensions. Key contributions include the extension to the governing equation in section A and the development of restricted surface as an efficient geometry and topology marching procedure in 3 dimensions in section B. Section III displays parameterised surfaces using the 3D-RSVS. These include a study of the geometric and topological behaviours of the new parameterisation. Surfaces of aerodynamic interest are also presented.

II. Restricted surfaces volume of solid for 3-dimensional aerodynamic parameterisation

The role of the parameterisation method is to provide an interface between an optimisation method and a physical model to form a shape optimisation framework. Efficiency and flexibility of shape optimisation frameworks limited by the geometric capability of the parameterisation method. Previous work by the authors has led to the successful development of a 2-dimensional topologically flexible parameterisation for aerodynamics [33]. The 3-dimensional parameterisation proposed in this work is the natural extension of the existing RSVS, for this reason discussion of features of the new parameterisation is done through 2-dimensional images. This section presents how the 3-dimensional restricted surface volume of solid (3D-RSVS) parameterisation translates sets of volume fraction design variables specified on a fixed grid into closed surfaces of varying topology. For optimisation frameworks to exploit the 3D-RSVS efficiently, this process must reliably produce smooth features at a resolution below the grid on which VOS values are defined.

To achieve this level of smooth control, the 3D-RSVS profile is defined as: the closed surface of minimum area

that will match the volumes of the design variables. It is built using a restricted surface (r-surface). The r-surface (e.g. in figure 5) is a method for "vertex marching" which allows efficient topology handling and is tolerant of any layout of VOS design variables. This description is the natural extension of the 2-dimensional formulation where the RSVS profile is defined as: the closed contour of minimum arc-length that will match the areas of the design variables. It is built using a restricted snake (r-snake).

This section develops the integration of the r-surface with the 3D-RSVS condition of minimising the area under volume constraints. This condition was found to reliably produce smooth profiles in 2-dimensions enabling a compact parameterisation. The 3D RSVS is implemented in C++, the code is made available by the authors on GitHub[a].

A. Governing equations of the RSVS

Maintaining smooth control close to topology changes is one of the main difficulties of the introduction of topological flexibility into aerodynamic parameterisation. Indeed, topology changes are geometrically discontinuous regions of the design space. This is addressed through the choice of governing equation which must allow topological transitions with minimal discontinuities. A set of volume of solid values are defined on a grid, superimposed on the design space. For an optimise the design variables become the fraction of each cell that shall be inside the parameterised shape. This process is shown for a simple 2 dimensional grid in figure 3. This parameterisation procedure provides intuitive handling of topology change without maintaining explicit control of it. It is important that topology is not controlled explicitly as this would require an heterogeneous set of design variables to achieve sufficient shape and topology control. This would certainly lead to severely discontinuous design spaces posing problems for the local and global optimisers used in aerodynamic optimisation. This approach would also be bespoke to the problem being tackled.

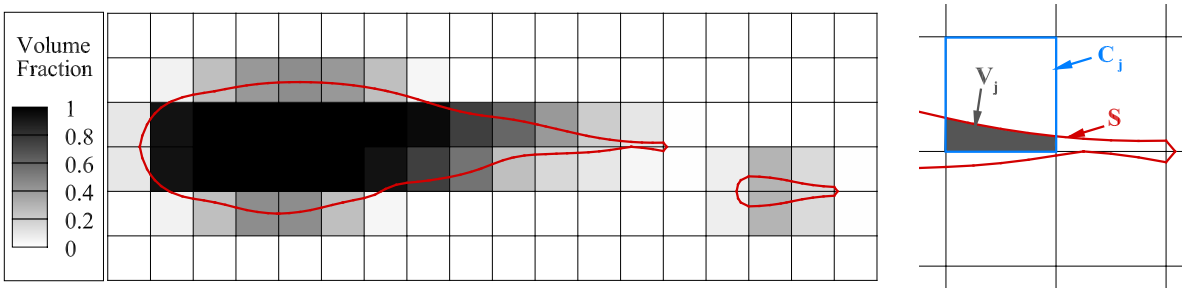

a) Volume of solid (VOS) design variables as grey-scale and RSVS profile in red; 1 corresponds to a completely full cell and 0 an empty cell.

b) VOS definitions for equation 1

Figure 3. Example RSVS profile and design grid with label definitions for the governing equation (eq. 1), the 2D-RSVS parameterisation is used for clarity of the images.

The VOS design variables do not include in themselves rules for building a profile. These rules must generate profiles which are continuous and smooth, allow features smaller than the VOS design variables, and be indifferent to the type of grid they are being applied to. This last requirement opens up the possibility of using non-cubic grids for improved flexibility and compactness of the method.

The 3-dimensional RSVS geometries are defined as the surface with the smallest area matching the VOS in every cell. The mathematical formulation of this problem is given in equation 1. This system is analogous to the effect of a tensile force "shrink-wrapping" the required VOS in each cell; the benefit is it allows for smooth profiles in most cases but can also recover sharp corners and edges where the VOS requires it. The general form of the 3-Dimensional RSVS problem is developed for a closed surface S which is constrained in m design cells (C_j) to have a specified volume fraction V_j. These variables are represented graphically in figure 3b for a 2 dimensional grid.

$$\begin{aligned} \min \quad & \iint_{S \to \mathbf{x}(t,u)} \left\| \frac{\partial \mathbf{x}}{\partial t} \times \frac{\partial \mathbf{x}}{\partial u} \right\| dt\, du \\ \text{s.t.} \quad & \iiint_{(S \cap C_j)} dx\, dy\, dz = V_j \qquad \forall j \in \{0, \cdots, m\} \end{aligned} \tag{1}$$

The rules above are the natural extension to 3-dimensions of the 2D-RSVS: the length minimisation has become a surface minimisation and the area constraints become volume constraints. As was the case in 2 dimensions the design

[a] https://github.com/payoto/rsvs3d

variables that control the surface are volume fractions specified in each cell of a *design grid*. This design grid is defined at the start of an aerodynamic topology optimisation procedure and remains unchanged throughout.

The VOS is taken as a constraint on the area enclosed in both the profile and each cell. The next sections detail how this mathematical program can be solved using restricted surfaces to produce an effective shape and topology parameterisation method.

B. Development of a Parametric Active Restricted Surface Method

Development of a 3-dimensional, volume of solid based, topologically flexible parameterisation requires an efficient method for evolving topologically complex geometries. The 2D-RSVS used restricted snakes, a type of parametric active contour developed by Bischoff et al. [29,34]. Previous work in the extension of parametric active contour methods to 3 dimensions have been successful, notably the development of topologically flexible T-surfaces by McInerney et al. [27] for medical image segmentation. This sub-section looks at extending the r-snake to evolve as a surface on 3-dimensional grids, basic information about r-snakes is presented in the paragraphs below (sec. C). For a complete guide for the implementation of restricted snakes the reader is referred to the original publication by Bischoff et al. [29,34].

1. *Vertex marching procedure*

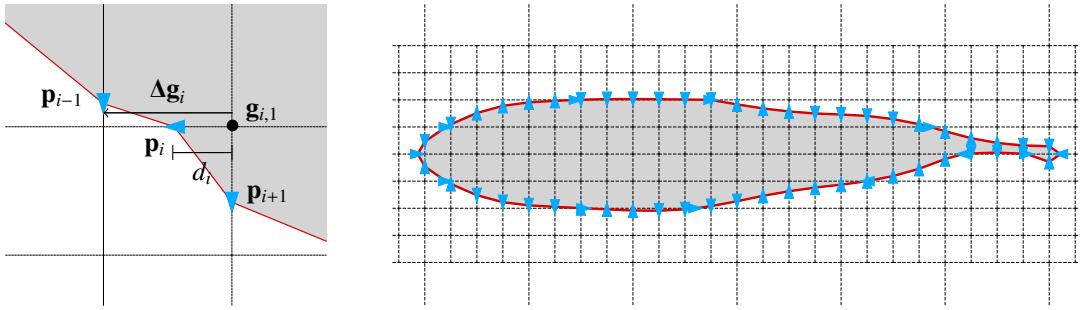

a) Close-up view of snake and snaxel **b) Full view of a closed r-snake**

Figure 4. R-snake contour (in red) with snaxels (in blue) evolving on the snaking grid (dashed line).

To build the RSVS parameterisation methods the restricted snake in 2D and the restricted-surface must be evolved until they solve the RSVS governing equation. To allow a high degree of geometric flexibility with few design variables, features need to be recovered below the resolution of the VOS grid. The restricted snake and surface are vertex marching procedures where the control points (called snaxels) are constrained to move on a predefined grid, as a consequence this snaking grid controls the number of snaxels and the resolution of the geometry. By marching the snake on a grid finer than the VOS grid, smooth features below the resolution of the volume design variables can be recovered.

Figure 4 shows an example r-snake and snaking grid as well as the variables associated with the snaxels. These variables are the same for a r-surface. Because snaxels are constrained to the grid, their position is entirely controlled by a single variable: the normalised distance d_i. This normalised distance can be updated using a chosen iterative behaviour. In the case of the RSVS the governing area minimisation (eq. 1) is adapted into a discrete formulation where these normalised distances are teh design variables.

For restricted snakes, the target object is a 1-dimensional line embedded in a 2-dimensional surface *snaking grid*. This line is composed of 0-dimensional vertices (called snaxels) which are constrained to move on the 1-dimensional edges of the *snaking grid*. The connectivity rules of the r-snakes were explained as follows [34]:

- No 2 connected snaxels can be on the same edge;
- Snaxels must travel out of the profile.

This second rule means that snaxels must be pointing from the inside of the profile to the outside, they cannot travel tangentially. The implication is that a snaxel cannot be connected by two edges which are part of the same face of the snaking grid.

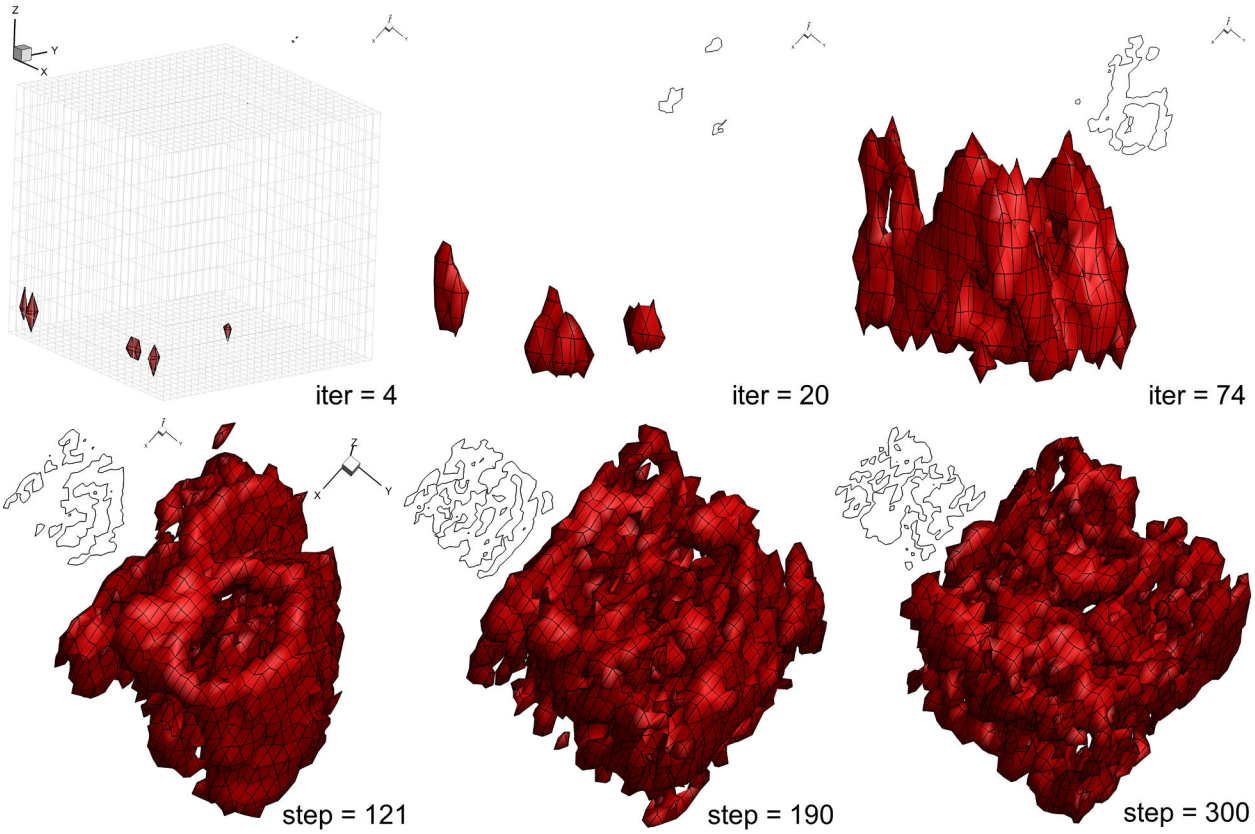

Figure 5. Test of the restricted surface process and rules: a restricted surface in a Cartesian snaking grid is evolved under a velocity field with random variations. The surface is in red, the black outlines are a section through the surface. The proposed restricted surface algorithm is robust and fast for arbitrary complex topologies.

Recognising that two connected r-snake edges cannot be part of the same face of the snaking grid, allows the rules of r-snakes to be extended to form a new parametric active surface restricted to move on a volume grid. The rules for this restricted-surface (r-surface) become:

- No 2 snaxels connected (by an edge) can be on the same *snaking grid* edge;
- No 2 r-surface edges connected (by a snaxel) can be in the same *snaking grid* face;
- No 2 r-surface faces connected (by r-surface edge) can be in the same *snaking grid* cell;

The 3-dimensional rules stated above can be further extended generalised to handle the marching of a N-dimensional restricted-polytope, including support for topology change. In all dimensions, there is a single special case for vertices which are 0-dimensional objects and all other rules are the same relative to the dimensionality of the object being handled. The N-dimensional rules are the following:

- No 2 restricted-polytope 0-dimensional object connected (by a restricted-polytope 1-dimensional object) can be on the same *snaking grid* 1-dimensional object;
- No 2 restricted-polytope z-dimensional object connected (by a restricted-polytope (z-1)-dimensional object) can be in the same *snaking grid* (z+1)-dimensional object for $z \in \{1, \cdots, N\}$;

The 3-dimensional rules were implemented into a C++ code and were shown to work robustly and efficiently for arbitrarily complex geometries evolved on a convex snaking-grid made of hexahedral cells. Figure 5 shows the evolution of a r-surfaces spawned from 6 distinct vertices, the velocity of the vertices along the edges is started at 1 and each step a random variation is added. Vertices that reach the edge of the snaking grid are reflected towards the

inside of the geometry. This was performed as a test of the topological flexibility of the r-surface process, validating it's use to evolve the 3D-RSVS surface.

The r-surface steps through snaking grid vertices by spawning a closed surface around the vertex and merging it with the approaching r-surface. It relies exclusively on connectivity information to detect collisions avoiding the need for expensive, floating point, intersection calculations. This process is efficient, robust and scalable thanks to the restricted nature of the parametric active surface.

2. *Triangulation of the R-Surface Solid into a Polyhedron*

While the rules for building the r-surface guarantee the formation of water-tight surfaces, it does not guarantee that the faces will be flat. This is because the r-surface is controlled by the positioning of its vertices with the rest of the geometry derived from the connectivity information forced by the snaking grid. Because flat surfaces are required for the reliable calculation of volume and area of the polyhedron, faces with more than 3 edges need to be triangulated. One of the most important considerations when choosing which triangulations will be used is the consistency of the area and volume of the triangulation with changes in connectivity which may only be minuscule changes in geometry.

To achieve this level of consistency and smoothness through changes in connectivity the triangulation of faces is built around point $\bar{\mathbf{c}}$ which is the mean position of a face's vertices normalised by edge length. Equation 2 shows this process for a closed face with $n+1$ vertices and the last vertex repeated.

$$\bar{\mathbf{c}} = \frac{\sum_{i=1}^{n} \|\mathbf{p}_{i+1} - \mathbf{p}_i\| \, (\mathbf{p}_{i+1} + \mathbf{p}_i)}{2 \sum_{i=1}^{n} \|\mathbf{p}_{i+1} - \mathbf{p}_i\|} \qquad \text{with} : \mathbf{p}_{n+1} = \mathbf{p}_1 \tag{2}$$

The r-surface face is then triangulated by linking this pseudo-centroid of the face to each of the vertices. This formulation is used as it prevents changes in connectivity, due to movements of the restricted surface, to cause jumps in the position of $\bar{\mathbf{c}}$; it is not affected by duplicate points.

C. Integration of the Restricted Surface with the Constrained Surface Minimisation

To drive the position of the restricted surface the original continuous area minimisation problem (eq. 1) is discretised in terms of the r-surface and snaxel variables, becoming the mathematical program of equation 7. This discretisation process needs six properties from the r-surface geometry and the snaxel positions. The first three of these properties are part of the movement algorithm; the last three properties of the snaxels are derived from connectivity and grid information, and are needed for the implementation of the discrete area minimization problem. These properties are: the snaxel index (i), used to reference it in all operations; the normalised position along an edge ($d_i \in [0,1]$); the scalar velocity along that edge ($v_i \in \mathbb{R}$); the snaxel position in Cartesian coordinates ($\mathbf{p}_i$); the direction of travel of the snaxel ($\mathbf{\Delta g}_i$) and the vertex of origin ($\mathbf{g_{i,1}}$); the normal vectors to the preceding and following edges ($\mathbf{n}_i$ and $\mathbf{n}_{i+1}$). These properties are represented graphically on figure 4a.

The continuous expressions presented in section A are easily computed for polyhedra with triangular faces. The area of each triangular face (S_k) is computed using equation 3, only the position of each of the corner vertices is required ($\mathbf{p_0}$, $\mathbf{p_1}$, $\mathbf{p_2}$). This approach is also applicable to $V_{S,k}$, the contribution of face k, to the volume of the polyhedron. The volume contributions from the underlying grid ($V_{C_j,k}$) are also taken into account. Vertices represented by a $\mathbf{p}_{i,k}$ are *active* vertices (snaxels or pseudo-centroids) which move with the surface being designed, *static* vertices which are part of underlying grids are represented by symbol $\mathbf{g}_{i,k}$.

$$A_{S,k} = \frac{1}{2} \left\| (\mathbf{p}_{1,k} - \mathbf{p}_{0,k}) \times (\mathbf{p}_{2,k} - \mathbf{p}_{0,k}) \right\| \tag{3}$$

$$V_{S,k} = \frac{1}{6} \left(\mathbf{p}_{0,k} \cdot \left((\mathbf{p}_{1,k} - \mathbf{p}_{0,k}) \times (\mathbf{p}_{2,k} - \mathbf{p}_{0,k}) \right) \right) \tag{4}$$

$$V_{C_j,k} = \frac{1}{6} \left(\mathbf{g}_{0,k} \cdot \left((\mathbf{g}_{1,k} - \mathbf{g}_{0,k}) \times (\mathbf{g}_{2,k} - \mathbf{g}_{0,k}) \right) \right) \tag{5}$$

The volume equations presented above can be assembled to calculate the volume of the polyhedron formed by the intersection of the r-surface and the faces of the *design grid*, this quantity is represented by value $V_{S,j}$.

$$V_{S,j} = \frac{1}{6} \sum_{k=j_S(1)}^{j_S(q_{jS})} \mathbf{p}_{0,k} \cdot ((\mathbf{p}_{1,k} - \mathbf{p}_{0,k}) \times (\mathbf{p}_{2,k} - \mathbf{p}_{0,k})) + \frac{1}{6} \sum_{k=j_C(1)}^{j_C(q_{jC})} \mathbf{g}_{0,k} \cdot ((\mathbf{g}_{1,k} - \mathbf{g}_{0,k}) \times (\mathbf{g}_{2,k} - \mathbf{g}_{0,k})) \tag{6}$$

$j_S(\{1, \cdots, q_{jS}\})$ and $j_C(\{1, \cdots, q_{jC}\})$ are indexing functions specified for each design cell selecting the correct vertices respectively from the triangulated r-surface and the volume grid. The equations for volume and area of the polyhedra formed by the intersection of the r-surface and the design grid have been derived and can now be substituted into the mathematical program which defines the RSVS problem in 3-dimensions (eq. 1). This process leads to equation 7 for the discrete RSVS problem applicable to triangulated r-surfaces.

$$\begin{aligned} &\min_{\mathbf{d}} \sum_{k=1}^{q} A_{S,k}\left(\mathbf{p}_{0,k}, \mathbf{p}_{1,k}, \mathbf{p}_{2,k}\right) \quad \text{with } \mathbf{p}_{i,k}\left(\mathbf{d}\right) \\ &\text{s.t.} \sum_{k=j_S(1)}^{j_S(q_{jS})} V_{S,k}\left(\mathbf{p}_{0,k}, \mathbf{p}_{1,k}, \mathbf{p}_{2,k}\right) + \sum_{k=j_C(1)}^{j_C(q_{jC})} V_{C,k}\left(\mathbf{g}_{0,k}, \mathbf{g}_{1,k}, \mathbf{g}_{2,k}\right) = V_j \end{aligned} \tag{7}$$

Building an RSVS surface consists in finding the positions $\mathbf{d}$ of the r-surface snaxels which solve the mathematical program of equation 7. As is the case in 2-dimensions the objective function and the constraint are readily differentiable. This is critical to solving the area minimisation governing equation as it allows the use of efficient gradient based optimisation method. While the area and volume could be differentiated by hand, the task would be tedious and error prone. The differentiation of $A_{S,k}$, and $V_{S,k}$ with regard to $\mathbf{p}_{i,k}$ was carried out for triangles using the MATLAB symbolic toolbox. This allows C code to be directly generated for the mathematical functions, ensuring that no mistake is made when calculating Jacobian and Hessian. The same process is followed for the derivatives of $\mathbf{p}_{i,k}$ and $\bar{\mathbf{c}}$ with regard to $\mathbf{d}$.

This formulation has the benefit of being very general, it can be tackled on an arbitrary volume grid with any underlying snaking grid with any optimisation method. This generality guarantees a high degree of flexibility in the range of shapes that can be represented. The following sub-sections show how this problem can be solved efficiently by using a Newton step sequential quadratic programming (SQP) procedure. The availability of analytical gradients for the surface area condition (the objective function) and the volume information (constraints) means a gradient based method may be applied efficiently.

D. Development of the SQP for snake marching

To solve this surface length minimisation a method was required that would converge in few iterations and function evaluations. For this reason a sensible choice is to use a gradient based method. The availability of analytical first and second derivatives means that sequential quadratic programming (SQP) is a viable option. A damped Newton step defined from a quadratic approximation to the full mathematical program is used to advance. The Newton step SQP equations presented below are derived in Boggs and Tolle [35] and were implemented by the authors into the 2-dimensional snaking process to calculate the velocity of the snaxels (v_i), the same approach is used in 3 dimensions. Only equation 8 for the update of the snaxel velocities is shown here. Derivation of it follows the cannonical form by Boggs and Tolle [35].

Updating the snaxel position is done by first calculating the Lagrange multipliers at the next step ($\mathbf{u}^{k+1}$) and using this result to update the vector of design variables $\mathbf{d}^{k+1}$.

$$\begin{aligned} \mathbf{u}^{k+1} &= \left(\left[\nabla_{\mathbf{d}}\mathbf{h}\right]^T \left[\mathbf{H}_{\mathbf{d}} f\right]^{-1} \left[\nabla_{\mathbf{d}} f\right]\right)^{-1} \left(\mathbf{h} - \left[\nabla_{\mathbf{d}}\mathbf{h}\right]^T \left[\mathbf{H}_{\mathbf{d}} f\right]^{-1} \left[\nabla_{\mathbf{d}} f\right]\right) \\ \Delta_{\mathbf{d}}^{k+1} &= \mathbf{d}^{k+1} - \mathbf{d}^{k} = -\left[\mathbf{H}_{\mathbf{d}} f\right]^{-1} \left(\left[\nabla_{\mathbf{d}} f\right] + \left[\nabla_{\mathbf{d}}\mathbf{h}\right] \mathbf{u}^{k+1}\right) \end{aligned} \tag{8}$$

The change in distances $\Delta_{\mathbf{d}}^{k+1}$ is used as the velocities (v_i) of the snaxels, letting the snaking process handle damping and connectivity changes. For the implementation of the SQP detailed above the terms of equation 8 must be computed, these are: the Jacobian of the constraints $[\nabla_{\mathbf{d}}\mathbf{h}]$; the gradient of the objective $[\nabla_{\mathbf{d}} f]$ and the Hessian of the objective $[\mathbf{H}_{\mathbf{d}} f]$. Thanks to the formulation of the snaking process all these values are available analytically by differentiating the appropriate area and snaxel position with respect to the design variable to the length minimisation program, the distances d_i. In both 2 and 3 dimensions the influence of each snaxel is limited to its direct neighbours, leading to sparse and easily invertible matrices.

E. SQP Sensitivity for Integration with Adjoint Solvers

The parametrised contour is the result of an optimisation method where the volume fraction is a constraint on the design (see equation 7). This formulation means the change in position of the profile due to a change in the volume fraction can be calculated analytically through a local sensitivity analysis. This approach means that the calculation

of derivatives benefits from a wealth of previous research into sensitivity analyses for SQP algorithms [36, 37]. Equations 9 and 10 show how results for the sensitivity analysis of non-linear programs from Buskens and Mauer [37] can be applied directly to the SQP of the RSVS to calculate the change in the r-surface due to small changes in VOS. This approach allows efficient integration of the RSVS in an adjoint based optimisation framework by providing a cheap way of calculating design sensitivities once a profile is generated.

$$\begin{pmatrix} \nabla_{\mathbf{V}}\mathbf{d} \\ \nabla_{\mathbf{V}}\mathbf{u} \end{pmatrix} = -\begin{pmatrix} \mathbf{H}_{\mathbf{d}}\mathcal{L} & \nabla_{\mathbf{d}}\mathbf{h}^T \\ \nabla_{\mathbf{d}}\mathbf{h} & \mathbf{0} \end{pmatrix}^{-1} \begin{pmatrix} \left(\nabla_{\mathbf{d}}^T\nabla_{\mathbf{V}}\right)\mathcal{L} \\ \nabla_{\mathbf{V}}\mathbf{h} \end{pmatrix} \tag{9}$$

$$\nabla_{\mathbf{V}}\mathbf{p}_i = \nabla_{\mathbf{V}}\left(d_i\Delta\mathbf{g}_i + \mathbf{g}_{i,1}\right) = \Delta\mathbf{g}_i\,\nabla_{\mathbf{V}}d_i \tag{10}$$

III. 3 Dimensional Parameterisation Results

This section presents profiles generated using the Restricted Surface method driven by the area minimisation, volume constrained SQP. First (sec. III.B), cases designed with a single and two volume of solid cells are shown. These are used to validate the implementation of the 3D-RSVS, to make sure that it does perform area minimisation of volume constrained surface. The smoothness resulting from the area minimisation is exploited to generate some standard aerodynamic bodies in section C. In section D surfaces highlighting the topological flexibility of 3D-RSVS on small layouts of Volume of Solid cells are shown.

A. Practical surface generation

The RSVS rules only specify how to evolve a surface but provide no guidance regarding the initialisation. For aerodynamic applications and more generally the design of external boundaries it is effective to start at the faces which touch a void and a non-empty volume cell. This provides fast convergence and intuitive behaviour to a designer. Internal voids can then be created if the restricted surface has failed to explore non-full volume cells.

B. Validation of the Restricted Snake Volume of Solid (RSVS) Parameterisation

Performance of aerodynamic optimisation frameworks is highly dependent on the behaviour and flexibility of the parameterisation method. To understand how the RSVS will perform in this context it is useful to explore the properties

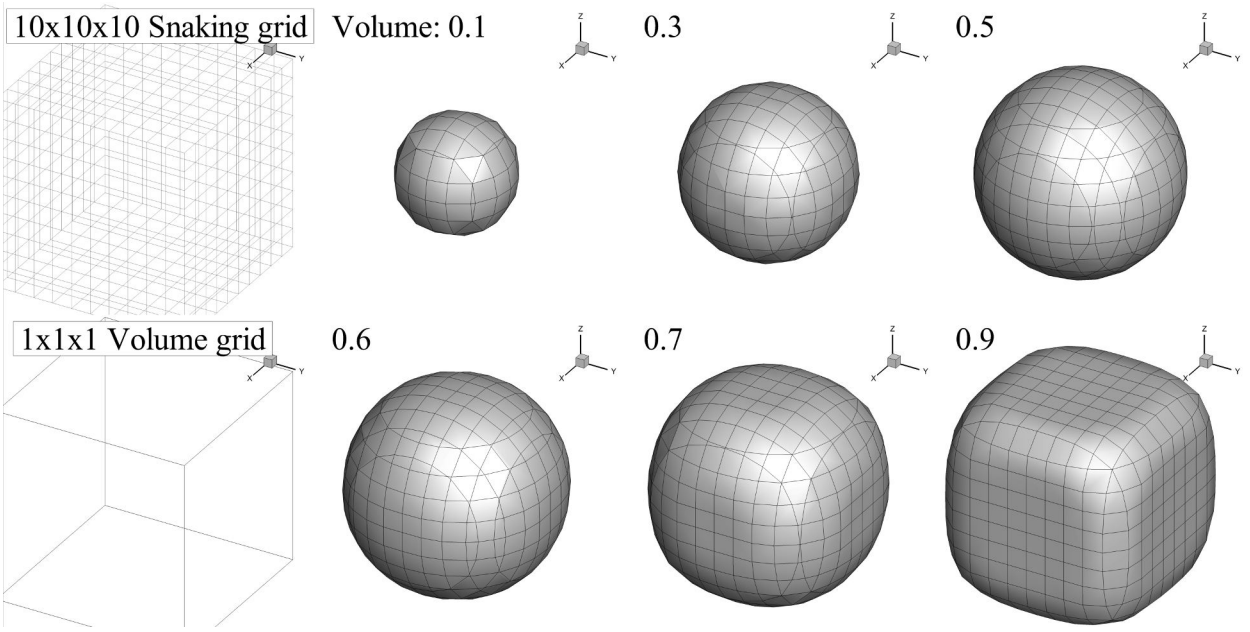

Figure 6. Geometries defined by a single volume cell with VOS from 0.1 to 0.9.

of the curves generated by the new method. The discrete constrained length minimisation which governs the behaviour of RSVS profiles can be expressed for an analytical continuous profile. This analytical formulation to the problem can be explored using calculus of variations and it can be shown that the 2D-RSVS forms piecewise continuous circular patches.

While an analytical study of the 3D-RSVS problem has not yet been performed it is natural to expect its behaviour to be similar: for shapes defined by few design variables the geometry should be spherical patches. To validate the implementation of the RSVS shapes designed with a single VOS cell were generated and are shown in figure 6. This single volume cell is refined into a 10^3 snaking grid. These shapes clearly show that the RSVS converges to spherical profiles up to volume fractions of 0.5. Beyond that volume fraction the surface is limited by the underlying grid on which the VOS are specified and starts to form a cuboid with round edges.

To suplement the qualitative observations from figure 6, the volume and area of 3D-RSVS bodies is compared to spheres of equivalent volume in table 1. The radius of the spheres is chosen to produce the same volume that is specified on the RSVS grid. Table 1 shows that for low value of requested volume fraction (up to 0.5) volume convergence is good ($\lessapprox 10^{-5}$). As the required VOS approaches 0.5 the area approaches that of a sphere, the area error dropping as low as 0.34% for a sphere of volume 0.5. This is expected: the 3D-RSVS's discretisation of the sphere depends on the number of intersections the geometry has with the background snaking mesh. As the object gets smaller, the number of intersections reduces and the discretisation becomes worse. This observation is confirmed by generating a sphere of volume 0.5 on a finer snaking grid with 24^3 cells. On this snaking grid the area match was even closer at 0.09% (table 1).

For higher volume spheres the diameter becomes larger than the size of the grid, leading to flat surfaces where the geometry encounters the boundary. This explains the rapid increase in the difference of area between spheres and 3D-RSVS geometries. The difference in volume convergence is due to the different treatment of snaxels at the edge of the design space. Indeed these cannot be treated as normal design variables for the area minimisation process as they cannot move further outwards but still must be free to move back inwards. A change to the solver of the quadratic program might be needed to support inequality constraints for those snaxels which can only move in one direction. Approaches similar to QPOPT (the internal quadratic solver of SNOPT) [38] are being investigated to improve convergence speed.

Table 1. Numerical comparison of the areas and volumes of 3D-RSVS geometries and spheres of the same target volume.

Figure	Design variables	Expected Sphere Properties			RSVS geometry		Error		Observation
		V	Diameter	Area	Volume	Area	Volume	Area	
fig. 6 upper-left	1	0.1	0.576	1.042	0.100	1.054	3.46E-13	-1.16%	
	1	0.2	0.726	1.654	0.200	1.672	3.23E-06	-1.08%	
fig. 6 upper-middle	1	0.3	0.831	2.167	0.300	2.176	-2.03E-07	-0.40%	
	1	0.4	0.914	2.625	0.400	2.638	2.62E-05	-0.48%	
fig. 6 upper-right	1	0.5	0.985	3.046	0.500	3.057	-2.45E-07	-0.34%	
fig. 6 lower-left	1	0.6	1.046	3.440	0.599	3.456	1.02E-03	-0.44%	at border
fig. 6 lower-middle	1	0.7	1.102	3.813	0.700	3.871	3.52E-04	-1.54%	at border
	1	0.8	1.152	4.168	0.798	4.362	2.03E-03	-4.66%	at border
fig. 6 lower-right	1	0.9	1.198	4.508	0.893	4.840	8.28E-03	-7.36%	at border
fig. 10 upper-middle	3	0.75	0.895	5.030	0.750	5.052	2.70E-04	-0.45%	2 spheres
	1	0.5	0.985	3.046	0.500	3.049	-1.04E-06	-0.09%	24^3 snaking grid

C. Generation of shapes of aerodynamic interest

In the previous section we showed the capability of the 3D-RSVS to accurately converge on a given volume fraction and the succesful implementation of the area constraint. Assembling more of these VOS design variables, smooth surfaces can be designed. As an initial test of the 3D-RSVS surfaces resembling aerodynamic surfaces were generated. The surfaces chosen were the Sears-Haack body, the truncated Sears-Haack body and a wing with aerofoil cross-sections.

Full and truncated Sears-Haack bodies were chosen to be presented as they are known analytical optima of the optimisation of drag under a volume constraints [39, 40]. The truncated ogives were shown to be optimal in 2 dimensions by Klunker and Harder [41] for values of area above 0.6 [30]. This case was used extensively by the authors to validate the 2D-RSVS and a similar process will be followed for the 3 dimensional parameterisation.

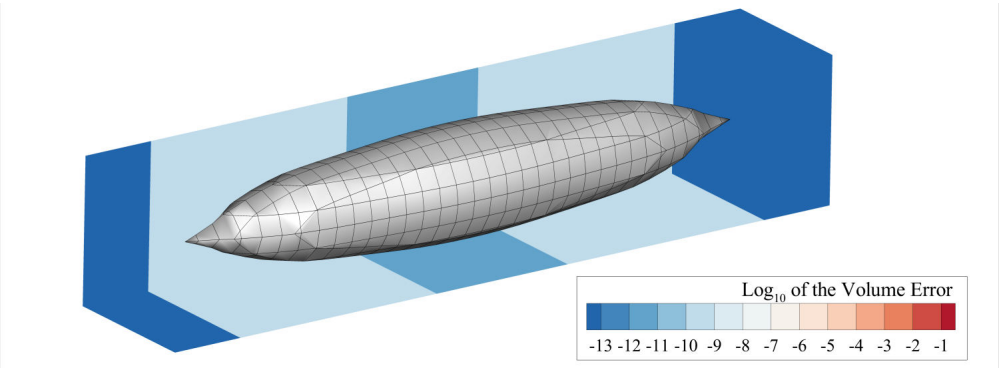

Figure 7. Sears-Haack body represented using 40 VOS cells in [2, 2, 10] layout. The colour in the colours in the background present the level of convergence of the r-surface on the correct volume.

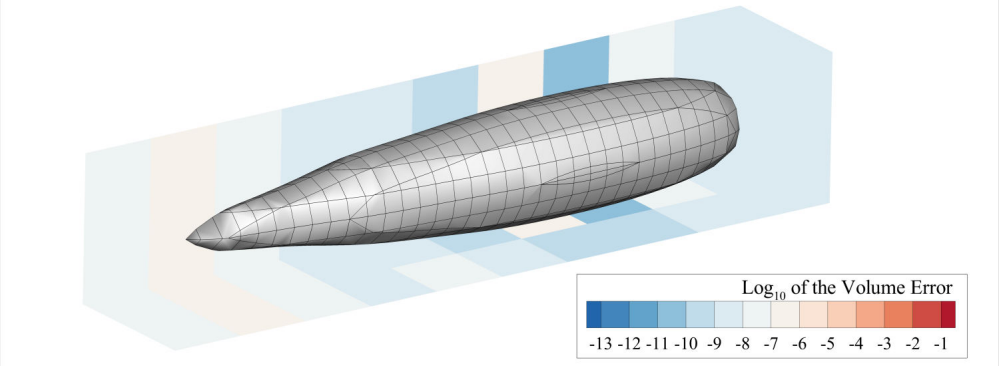

Figure 8. Truncated Sears-Haack body represented using 40 VOS cells in [2, 2, 10] layout. The colour in the colours in the background present the level of convergence of the r-surface on the correct volume.

Figure 7 shows a Sears-Haack body, and the truncated Sears-Haack body is presented in figure 8. These surfaces use a [10, 2, 2] layout of VOS cells and 4^3 snaking refinement. As was the case in 2 dimensions the RSVS produces mostly smooth profiles but can be forced to produce a sharp corner or a sharp edge by using small volume fractions, providing accurate positionning of the leading and trailing edges. The volume convergence information shown on the background volume mesh show that the volume fractions can be matched with precision by the RSVS process.

Drag minimisations of wings are common cases within the aerodynamic shape optimisation community [42, 43]. Figure 9 presents a coarse representation of a wing using a [2,5,6] layout of design variables. This provides 10 volume fraction values to design the cross-section of the wing at six span locations. One of the side effects of building surfaces of minimum area is that long and slender profiles are not initially possible. To allow elongated bodies, the long dimension of the surface needs to be de-weighted in terms of area. This can be achieved either inside the shape generation by multiplying the coordinates by individual weights or by externally altering the aspect ratio of the grid.

Three dimensional optimisation cases often rely on deformative methods starting from a high quality model. This presents a challenge in evaluating the RSVS: as a constructive parameterisation method it cannot easily exploit the benefit of an existing geometry. To achieve high fidelity parameterisation and optimisation hierarchical design variables have been shown to allow optimisation of aerodynamic features at a wide range of geometric scales [32, 44]. Another possible approach to achieve a very high resolution of the geometric surface is to use a hybrid parameterisation approach. This uses a very efficient local parameterisatin method after the topology parameterisation performed by the RSVS. The authors previously integrated the 2D-RSVS with the multi-level subdivision curves developed by Masters et al. [32] and achieved significant improvements compared to both isolated frameworks [45]. A similar approach is being considered in 3 dimensions. Finally the RSVS can be used to represent only part of a geometry allowing the optimisation of a smaller element of a high quality model. This approach could be extended to the meshing to use overset meshes a method succesfully used in ASO for complex geometries [46, 47]. Despite these possibilities, wing design is not the primary use case of the RSVS: the RSVS will be targeted at cases where its topological flexibility, is an asset not a drawback.

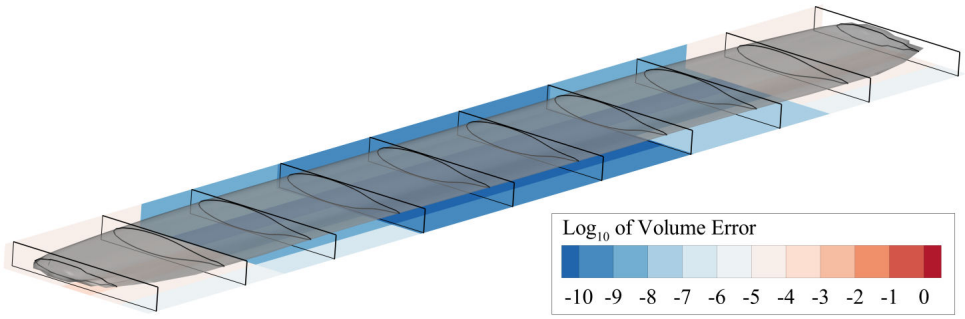

Figure 9. Coarse wing represented using 60 VOS cells in [2, 5, 6] layout. The colour in the colours in the background present the level of convergence of the r-surface on the correct volume.

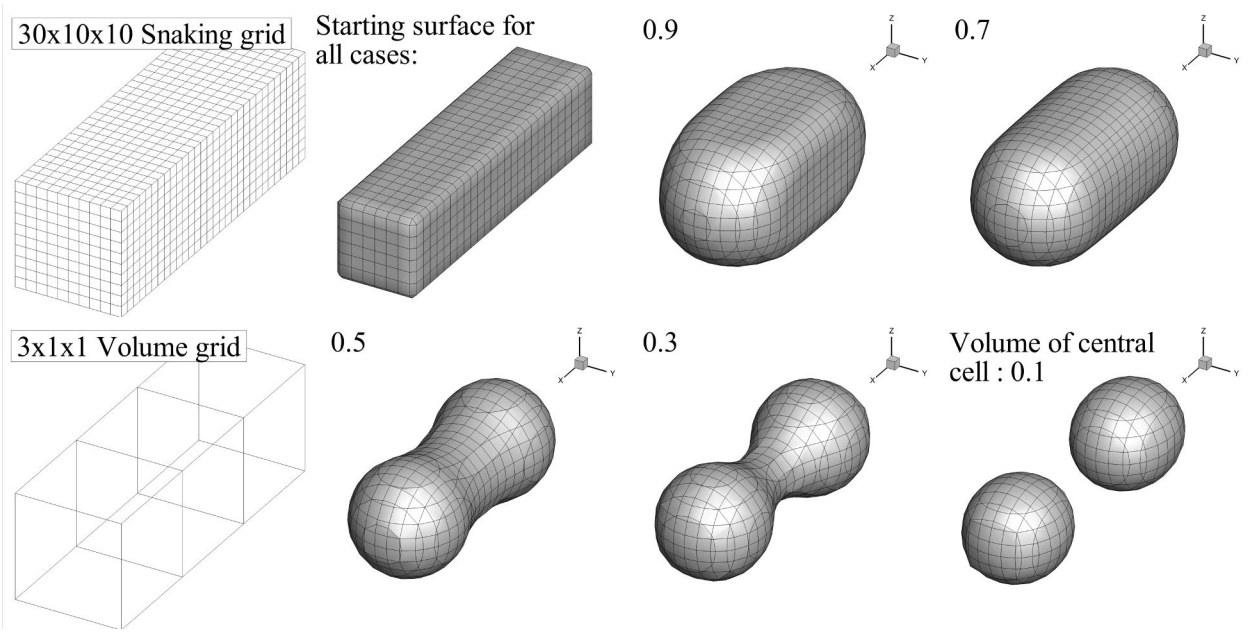

Figure 10. 5 different final geometries defined by 3 volume cells. The VOS in the cells at the ends of the body is kept constant while the volume fraction of the central cell is varied from 0.1 to 0.9.

D. Topological flexibility of the 3 dimensional RSVS

The minimal case to show the topological behaviour of the 3D-RSVS requires 3 VOS cells. Figure 10 presents the geometries generated by varying the value of the central VOS cell. Between values of 0.3 and 0.1 the topology of the geometry changes from a single body to 2 spherical bodies. The case generating two spheres is added to table 1 and shows a similar geometric convergence on spheres as the cases discussed in the previous section (B).

Figure 11 shows 4 different surfaces generated by the 3 dimensional RSVS. On the left the volume grid on which the volume fractions are specified (thick lines) and the snaking grid (thin lines) on which the restricted surface evolves. These surfaces illustrate some of the more complex topologies that can be achieved with a small set of design variables. While these topologies may not be of interest for external aerodynamic optimisation, these could have application in the design of pipes or structures.

IV. Automatic Design of Volume of Solid grids

One of the drawbacks of the two and three dimensional RSVS parameterisation methods is that a regular Cartesian VOS grid contains much less implicit information about aerodynamic problems compared to traditional parameterisation methods. The RSVS, while being more general than other parameterisations, also requires careful setup of the design variable layout to tackle an optimisation problem efficiently. To avoid this a procedure for the VOS grid

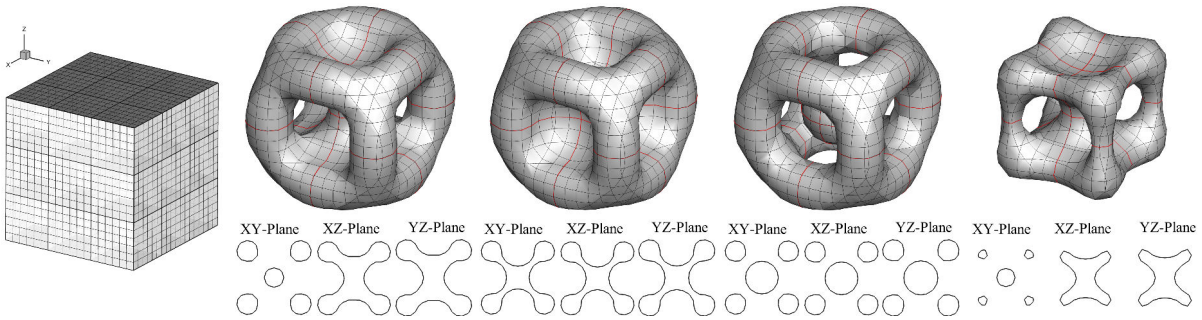

Figure 11. Four different final geometries defined by 27 VOS cells in a 3^3 layout. On the left the volume and snaking grid on which they are defined. These cases illustrate the topological and smooth shape control 3D-RSVS provide with few design variables. To aid understanding of the topologies being represented slices through the centre of each dimension are provided.

to be automatically designed during an optimisation is presented. This hierarchical approach to the design variables removes the need for the careful manual design of the grid.

These approaches start an optimisation problem with few design variables, this allows large but coarse changes to the design. As this process converges additional design variables are added allowing progressively finer and smaller scale changes to the design to be added. Hierarchical approaches by Anderson and Aftosmis [31] and Masters et al. [48] have accelerated and improved convergence on complex aerodynamic optimisation problems. Similar approaches have been succesfully exploited in structural topology optimisation by Kim et al. to improve the performance of agent based optimisers [49] and by Bandara et al. to build a mutli-resolution framework based on sequential shape and topology optimisation using subdivision curves [50]. Similar ideas have been used in structural topology optimisation by Kim et al. to improve the performance of agent based optimisers [49]. The RSVS lends itself to such hierarchical approaches, the refinement of design VOS design variables is intuitive and exact.

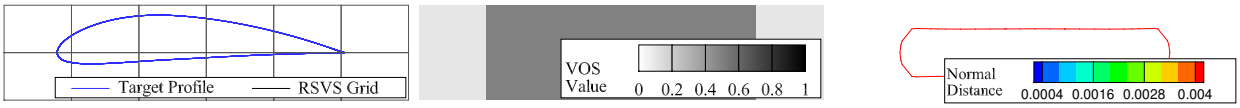

a) Start of refinement step 0 for the NACA4412 geometric design (iteration 1)

b) End of refinement step 6 for the NACA4412 geometric design (iteration 169)

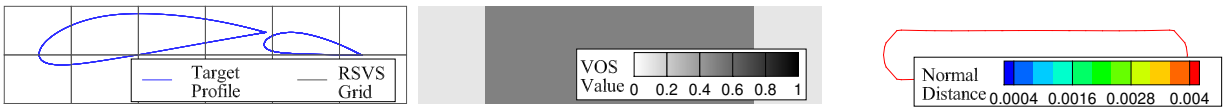

c) Start of step 0 for the geometric design a multi body airfoil (iteration 1)

d) End of refinement step 8 for the geometric design a multi body airfoil (iteration 136)

Figure 12. Geometric recovery of a NACA4412 and a multi-body airfoil using up to 8 refinement steps; with the RSVS grid and the target profile (left), the VOS values for the geometry (centre) and the corresponding profile coloured according to its normal distance to the target profile (right) at the first and final iterations.

The local refinement scheme developed for the RSVS relies on the parameterisation's ability to generate profiles using volume of solid defined on arbitrary polygonal grids. The initial set of cell in the VOS grid is progressively split in regions of the design space where the profile exhibits high curvature. This allowes high fidelity control of the geometry without penalising early convergence or requiring manual design of the RSVS grid. A detailed description of

the local refinement scheme is beyond the scope of this paper but can be found in the authors' previous publication [30].

Example results of the RSVS with refinement are shown in figure 12. The refinement process was tested on the geometric inverse design of a single body and a multi-body aerofoil, using a conjugate gradient optimiser. The goal of this test is to explore the flexibility of the method and the quality of the integration with the optimiser. The two cases were tackled with 8 refinement steps starting from a coarse grid of 2 by 6 design variables, the grid at the first and final refinement step is shown in figure 5 along with the corresponding profile and volume fractions.

The set-up of this case was done to test the effectiveness and flexibility of the RSVS parameterisation with local refinement. For this reason the profile was allowed to evolve freely over the grid with no constraint on the position of leading edge and trailing edges. The final profiles (fig. 12b and 12d) show the parameterisation successfully built a smooth leading edges and sharp trailing edges a. What this case demonstrates is the ability of local refinement to tune the RSVS parameterisation to the optimisation case being tackled without any intervention from the designer. Useful in 2 dimensions, this ability to adapt to the case at hand is critical to being effective in 3-dimensions, as designing the perfect RSVS grid for a case with an unknown solution will be even harder.

V. Conclusion & Future work

In this paper the restricted snake volume of solid parameterisation was extended to 3 dimensional surfaces. The 3D-RSVS is very conceptually similar to the it's 2 dimensional sibling. This allowed a straight-forward development and to maintain many of the desirable geoemtric properties of the RSVS. The 3D RSVS is shown to be capable of representing complex topologies as well as smooth aerodynamic shapes using a compact set of design variable. This parameterisation also has the added benefit of being intuitive to a designer, the geometric design variables being easily interpretible and the contour generation having a predictable behaviour.

Development of the 3D-RSVS requrired the extension of the governing equations. This proved conceptually straight forward and the behaviour of the surfaces generated using the area minimisation objective is very similar to that of the 2 dimensional parameterisation. The implementation of the parameterisation also required the extension of the restricted-snakes process. This was succesfull yielding an extremely robust and scalable geometry and topology marching procedure relying entirely on connectivity and integer arithmetics. These combined developments were shown to produce parameterisation of smooth shapes with topological flexibility for arbitrary surfaces. To avoid the complexity of manually designing VOS design variable layouts an automatic method for this process is presented. This process has already been shown to work in 2 dimensions and extends naturally to 3 dimensions.

The priority is now on integrating this parameterisation into an optimisation framework. The 3-dimensional RSVS is being included into a modular optimisation framework that was first developed for the 2D RSVS parameterisation method [33]. This framework is being extended to support 3 dimensional geometries by supporting automatic meshing using TetGen, a quality tetrahedral mesh generator and a 3D Delaunay triangulator [51], solved with the Stanford University Unstructured (SU^2) [52] flow solver. Local and global optimisation will be included in the form of conjugate gradien SNOPT [38] and differential evolution. A number of objective functions are being integrated to provide benchmarking of the parameterisation at reasonable cost.

To test the effectiveness of the 3-dimensional aerodynamic topology parameterisation outlined in this paper, the drag minimisations of inviscid, supersonic, constant area optimisations will be used. Similar cases were tackled in 2-dimensions using the RSVS method with great success, highlighting the potential of topological optimisation to discover new designs [30, 33, 45]. Beyond its application in optimisation the 3D-RSVS's topological flexiblity and intuitiveness could be used for the rapid generation of 3 dimensional models for computer graphics and design.

Acknowledgements

This work was carried out using the computational facilities of the Advanced Computing Research Centre, University of Bristol - http://www.bris.ac.uk/acrc/. Funding: This work was supported by the EPSRC Research Council UK and the University of Bristol through DTP grant EP/M507994/1. All the data needed to support the conclusions of this article are presented in the paper.

References

[1] Vassberg, J. C. and Jameson, A., "Industrial Applications of Aerodynamic Shape Optimization," Tech. rep., Brussels, 2014.

[2] Hunter, E., "Alternate Detail Part Design and Analysis: Topology, Size, and Shape Optimization of CH-47 Chinook Underfloor Structure," *62nd ANNUAL FORUM PROCEEDINGS-AMERICAN HELICOPTER SOCIETY*, Vol. 1, AMERICAN HELICOPTER SOCIETY, INC, 2006, pp. 260–264.

[3] Deaton, J. D. and Grandhi, R. V., "A survey of structural and multidisciplinary continuum topology optimization: post 2000," *Struct Multidisc Optim*, Vol. 49, 2014, pp. 1–38.

[4] Bendsøe, M. P. and Sigmund, O., "Material interpolation schemes in topology optimization," *Archive of Applied Mechanics (Ingenieur Archiv)*, Vol. 69, No. 9-10, nov 1999, pp. 635–654.

[5] Rozvany, G. I. N., "A critical review of established methods of structural topology optimization," *Structural and Multidisciplinary Optimization*, Vol. 37, No. 3, jan 2009, pp. 217–237.

[6] Sobieczky, H., "Geometry Generator for CFD and Applied Aerodynamics," *New Design Concepts for High Speed Air Transport*, Springer Vienna, Vienna, 1997, pp. 137–157.

[7] Kulfan, B. and Bussoletti, J., ""Fundamental" Parameteric Geometry Representations for Aircraft Component Shapes," *11th AIAA/ISSMO Multidisciplinary Analysis and Optimization Conference*, Vol. 1, American Institute of Aeronautics and Astronautics, Reston, Virigina, sep 2006, pp. 547–591.

[8] Sobieczky, H., *Parametric Airfoils and Wings*, chap. Parametric, Vieweg+Teubner Verlag, Wiesbaden, 1998, pp. 71–87.

[9] Hicks, R. M. and Henne, P. A., "Wing Design by Numerical Optimization," *Journal of Aircraft*, Vol. 15, No. 7, jul 1978, pp. 407–412.

[10] J. Toal, D. J., Bressloff, N. W., Keane, A. J., and E. Holden, C. M., "Geometric Filtration Using Proper Orthogonal Decomposition for Aerodynamic Design Optimization," *AIAA Journal*, Vol. 48, No. 5, 2010, pp. 916–928.

[11] Poole, D. J., Allen, C. B., and Rendall, T. C. S., "Metric-Based Mathematical Derivation of Efficient Airfoil Design Variables," *AIAA Journal*, Vol. 53, No. 5, may 2015, pp. 1349–1361.

[12] Chauhan, D., Chandrashekarappa, P., and Duvigneau, R., "Wing shape optimization using FFD and twist parameterization," *12th Aerospace Society of India CFD Symposium*, Bangalore, 2010.

[13] Allen, C. B. and Rendall, T. C. S., "CFD-based optimization of hovering rotors using radial basis functions for shape parameterization and mesh deformation," *Optimization and Engineering*, Vol. 14, No. 1, mar 2013, pp. 97–118.

[14] Vassberg, J. C., Harrison, N. A., Roman, D. L., and Jameson, A., "A Systematic Study on the Impact of Dimensionality for a Two-Dimensional Aerodynamic Optimization Model Problem," *29th AIAA Applied Aerodynamics Conference*, No. 3176, Honolulu, Hawaii, 2011, pp. 1–19.

[15] Castonguay, P. and Nadarajah, S., "Effect of Shape Parameterization on Aerodynamic Shape Optimization," *45th AIAA Aerospace Sciences Meeting and Exhibit*, No. January, American Institute of Aeronautics and Astronautics, Reston, Virigina, jan 2007, pp. 1–20.

[16] Masters, D. A., Taylor, N. J., Rendall, T. C. S., Allen, C. B., and Poole, D. J., "A Comparative Assessment of Aerofoil Parameterisation Methods for Aerodynamic Shape Optimisation," *SciTech*, San Diego, 2016, pp. 1–35.

[17] Masters, D. A., Poole, D. J., Taylor, N. J., Rendall, T., and Allen, C. B., "Impact of Shape Parameterisation on Aerodynamic Optimisation of Benchmark Problem," *54th AIAA Aerospace Sciences Meeting, AIAA SciTech Forum, (AIAA 2016-1544)*, American Institute of Aeronautics and Astronautics, Reston, Virginia, jan 2016, pp. 1–14.

[18] Bendsøe, M. P. and Kikuchi, N., "Generating optimal topologies in structural design using a homogenization method," *Computer Methods in Applied Mechanics and Engineering*, Vol. 71, No. 2, nov 1988, pp. 197–224.

[19] Kreissl, S., Pingen, G., Evgrafov, A., and Maute, K., "Topology optimization of flexible micro-fluidic devices," *Structural and Multidisciplinary Optimization*, Vol. 42, No. 4, oct 2010, pp. 495–516.

[20] Deng, Y., Liu, Z., Zhang, P., Liu, Y., and Wu, Y., "Topology optimization of unsteady incompressible NavierStokes flows," *Journal of Computational Physics*, Vol. 230, No. 17, jul 2011, pp. 6688–6708.

[21] Yoon, G. H., "Topology optimization for turbulent flow with SpalartAllmaras model," *Computer Methods in Applied Mechanics and Engineering*, Vol. 303, may 2016, pp. 288–311.

[22] CHEN, C., YAJI, K., YAMADA, T., IZUI, K., and NISHIWAKI, S., "Local-in-time adjoint-based topology optimization of unsteady fluid flows using the lattice Boltzmann method," *Mechanical Engineering Journal*, Vol. 4, No. 3, 2017, pp. 17–00120–17–00120.

[23] Wang, M. Y., Wang, X., and Guo, D., "A level set method for structural topology optimization," *Computer Methods in Applied Mechanics and Engineering*, Vol. 192, No. 1-2, jan 2003, pp. 227–246.

[24] van Dijk, N. P., Maute, K., Langelaar, M., and van Keulen, F., "Level-set methods for structural topology optimization: a review," *Structural and Multidisciplinary Optimization*, Vol. 48, No. 3, sep 2013, pp. 437–472.

[25] Hall, J., Rendall, T., Allen, C., and Poole, D., "A volumetric geometry and topology parameterisation for fluids-based optimisation," *Computers & Fluids*, Vol. 148, apr 2017, pp. 137–156.

[26] Hall, J., S. Rendall, T. C., and Allen, C. B., "Optimisation using smoothed particle hydrodynamics with volume-based geometry control," *Structural and Multidisciplinary Optimization*, 2017.

[27] McInerney, T. and Terzopoulos, D., "T-snakes: topology adaptive snakes." *Medical image analysis*, Vol. 4, No. 2, 2000, pp. 73–91.

[28] Delgado-Gonzalo, R., Uhlmann, V., Schmitter, D., and Unser, M., "Snakes on a Plane: A perfect snap for bioimage," *IEEE Signal Processing Magazine*, Vol. 32, No. 1, 2015, pp. 41–48.

[29] Kobbelt, L. P. and Bischoff, S., "Parameterization-free active contour models with topology control," *The Visual Computer*, Vol. 20, No. 4, jun 2004, pp. 217–228.

[30] Payot, A. D., Rendall, T., and Allen, C. B., "Mixing and Refinement of Design Variables for Geometry and Topology Optimization in Aerodynamics," *35th AIAA Applied Aerodynamics Conference, AIAA AVIATION Forum, (AIAA 2017-3577)*, No. June, American Institute of Aeronautics and Astronautics, Reston, Virginia, jun 2017, pp. 1–24.

[31] Anderson, G. R. and Aftosmis, M. J., "Adaptive Shape Control for Aerodynamic Design," *56th AIAA/ASCE/AHS/ASC Structures, Structural Dynamics, and Materials Conference*, American Institute of Aeronautics and Astronautics, Reston, Virginia, jan 2015.

[32] Masters, D. A., Taylor, N. J., Rendall, T. C. S., and Allen, C. B., "Multilevel Subdivision Parameterization Scheme for Aerodynamic Shape Optimization," *AIAA Journal*, Vol. 55, No. 10, oct 2017, pp. 3288–3303.

[33] Payot, A. D., Rendall, T., and Allen, C. B., "Restricted Snakes: a Flexible Topology Parameterisation Method for Aerodynamic Optimisation," *55th AIAA Aerospace Sciences Meeting, AIAA SciTech Forum, (AIAA 2017-1410)*, American Institute of Aeronautics and Astronautics, Reston, Virginia, jan 2017.

[34] Bischoff, S. and Kobbelt, L. P., "Snakes with topology control," *Image Rochester NY*, 2003, pp. 10.

[35] Boggs, P. T. and Tolle, J. W., "Sequential Quadratic Programming," *Acta Numerica*, Vol. 4, jan 1995, pp. 1–51.

[36] Fiacco, A. V. and Ishizuka, Y., "Sensitivity and stability analysis for nonlinear programming," *Annals of Operations Research*, Vol. 27, No. 1, dec 1990, pp. 215–235.

[37] Buskens, C. and Maurer, H., "SQP-methods for solving optimal control problems with control and state constraints: Adjoint variables, sensitivity analysis and real-time control," *Journal of Computational and Applied Mathematics*, Vol. 120, 2000, pp. 85–108.

[38] Gill, P. E., Murray, W., and Saunders, M. a., "SNOPT: An SQP Algorithm for Large-Scale Constrained Optimization," *SIAM Journal on Optimization*, Vol. 12, No. 4, jan 2002, pp. 979–1006.

[39] Sears, W. R., "On Projectiles of Minimum Wave Drag," *Quarterly of Applied Mathematics*, Vol. 4, No. 4, 1947, pp. 361–366.

[40] Haack, W., *Projectile Shapes for Smallest Wave Drag*, Graduate Division of Applied Mathematics, Brown University, 1948.

[41] Klunker, E. B. and Harder, K., "Comparison of Supersonic Minimum-Drag Airfoils Determined By Linear and Nonlinear Theory," Tech. Rep. February, NATIONAL AERONAUTICS AND SPACE ADMINISTRATION HAMPTON VA LANGLEY RESEARCH CENTER, Washington, 1952.

[42] Burdette, D. A. and Martins, J. R., "Design of a transonic wing with an adaptive morphing trailing edge via aerostructural optimization," *Aerospace Science and Technology*, Vol. 81, oct 2018, pp. 192–203.

[43] Khosravi, S. and Zingg, D. W., "Aerostructural Optimization of Drooped Wings," *Journal of Aircraft*, dec 2017, pp. 1–8.

[44] Masters, D. A., Taylor, N. J., Rendall, T., and Allen, C. B., "Three-Dimensional Subdivision Parameterisation for Aerodynamic Shape Optimisation," *55th AIAA Aerospace Sciences Meeting*, , No. January, 2017, pp. 1–17.

[45] Kedward, L. J., Payot, A. D. J., Rendall, T. C. S., and Allen, C. B., "Efficient Multi-Resolution Approaches for Exploration of External Aerodynamic Shape and Topology," *36th AIAA Applied Aerodynamics Conference*, American Institute of Aeronautics and Astronautics, June 2018.

[46] Kenway, G. K., Mishra, A., Secco, N. R., Duraisamy, K., and Martins, J., "An Efficient Parallel Overset Method for Aerodynamic Shape Optimization," *58th AIAA/ASCE/AHS/ASC Structures, Structural Dynamics, and Materials Conference*, American Institute of Aeronautics and Astronautics, Reston, Virginia, jan 2017.

[47] Secco, N. R. and Martins, J. R. R. A., "RANS-Based Aerodynamic Shape Optimization of a Strut-Braced Wing with Overset Meshes," *Journal of Aircraft*, sep 2018, pp. 1–11.

[48] Masters, D. A., Taylor, N. J., Rendall, T., and Allen, C. B., "A Locally Adaptive Subdivision Parameterisation Scheme for Aerodynamic Shape Optimisation," *34th AIAA Applied Aerodynamics Conference*, American Institute of Aeronautics and Astronautics, Reston, Virginia, jun 2016, p. 3866.

[49] Kim, I. Y. and De Weck, O. L., "Variable chromosome length genetic algorithm for progressive refinement in topology optimization," *Structural and Multidisciplinary Optimization*, Vol. 29, No. 6, 2005, pp. 445–456.

[50] Bandara, K., Rüberg, T., and Cirak, F., "Shape optimisation with multiresolution subdivision surfaces and immersed finite elements," *Computer Methods in Applied Mechanics and Engineering*, Vol. 300, mar 2016, pp. 510–539.

[51] Si, H., "TetGen, a Delaunay-Based Quality Tetrahedral Mesh Generator," *ACM Transactions on Mathematical Software*, Vol. 41, No. 2, feb 2015, pp. 1–36.

[52] Economon, T. D., Alonso, J. J., Albring, T. A., and Gauger, N. R., "Adjoint Formulation Investigations of Benchmark Aerodynamic Design Cases in SU2," *35th AIAA Applied Aerodynamics Conference*, , No. June, 2017, pp. 1–13.